Impact of Optimal Fuel Cell Management System on Fuel Cell Hybrid Electric Vehicle Efficiency

Yakoub ZINE[1], Amel BENMOUNA[1,3], Mohamed BECHERIF[1], Daniel HISSEL[2], *Fellow*, IEEE.

***Abstract*— Fuel cell hybrid electric vehicles (FCHEVs) play an important role in driving the transition towards more environment-friendly transportation and electric mobility. Their powertrain efficiency hinges on the effective distribution of power demands between the fuel cell (FC) and the battery, facilitated by an Energy Management System (EMS). In the literature, diverse strategies are utilized to handle the power allocation within the FCHEV. Unlike existing work, this paper breaks new ground by incorporating a Fuel Cell Management System (FCMS) into the EMS. This FCMS improves FC performance by simultaneously monitoring FC operational conditions: temperature and oxygen excess ratio. The proposed optimal FCMS is combined with the Nonlinear Model Predictive Control (NMPC) EMS and simulated across urban, suburban, and highway driving scenarios. The simulation results demonstrate the effectiveness of the proposed method, by achieving up to 4% enhancement in the overall efficiency.**

***Index Terms*— Fuel Cell Hybrid Electric Vehicle, Energy Management System, Nonlinear Model Predictive Control, Fuel Cell Management System.**

I. Introduction

The quest for a sustainable transportation sector is being paved by fuel cell hybrid electric vehicles (FCHEVs) due to their zero-emission capabilities [1]. The architecture of a FCHEV typically centers around a proton exchange membrane fuel cell, henceforth designated as the FC, as the primary power source. This FC is complemented by a battery as a supplementary source, forming a hybrid configuration that capitalizes on the strengths of both technologies [2].

The energy management system (EMS), a high-level controller in FCHEV, optimizes power flow and transitions between different sources [3]. EMS employs strategies, from rule-based to learning-based approaches, including notable examples such as State Machine Control (SMC) [4], Equivalent Consumption Minimization Strategy (ECMS) [5], Reinforcement Learning (RL) [6], etc. For real-time and online control, Model Predictive Control (MPC) is a preferred option due to its versatility in handling multiple constraints simultaneously [7]. Nonlinear MPC (NMPC), a variant of MPC, deals with complex nonlinear systems and optimizing custom cost functions with both linear and nonlinear constraints. In [8], an experimental implementation of NMPC was conducted using a FCHEV real-time hardware-in-the-loop setup. Despite its computational demands, NMPC successfully achieved reductions in hydrogen consumption and mitigated FC degradation when compared to linear MPC. In [9], a comprehensive overview is presented regarding the design and application of different types of MPC-based EMS for hybrid electric vehicles. The effectiveness of the EMS strategies has been widely demonstrated, but their scope is restricted to electric power management, leaving out consideration of FC operating conditions.

The optimization of the operating conditions, with a specific focus on temperature and air flow rate, relies on the accurate design and control of the auxiliary subsystems [10], often referred to as the Balance of Plant (BoP). The BoP encompasses vital auxiliary subsystems essential for FC operation, including hydrogen storage and supply, air supply, cooling system, water management system, and power electronics. In a FC system, the BoP can draw up to 20% of the gross power, thus leading to a decrease in overall efficiency [11]. To limit this efficiency loss and maintain peak performance, the implementation of a refined fuel cell management system (FCMS) becomes imperative. In [12], a dual loop coordinated management has been proposed to enhance the net power of a FC system, the results have shown an improvement of about 6% comparing to a manual guided control. In [13], it was demonstrated that optimizing both oxygen excess ratio and cathode pressure within the air system, identified as the primary energy consumer within the BoP, can result in a significant increase in efficiency of approximately 2% compared to conventional one-dimensional optimization.

This study investigates the impact of integrating an optimal FCMS into a NMPC-based EMS for a FCHEV. Unlike the other similar works, this control strategy is composed of three hierarchical levels: at the high-level, the EMS distributes electric power demand between sources, the mid-level focuses on optimizing FC system efficiency through operating condition adjustments, and the low-level ensures the control of the auxiliary subsystems.

The rest of this paper is organized as follows: the modeling of the hybrid system and the BoP is detailed in section II, the development of EMS and FCMS is addressed in Section III. Section IV carries out the simulation results and discussions. Conclusions and perspectives are drawn in Section V.

II. System structure and modeling

The global structure of the studied system is illustrated in Fig. 1.

**author contact:* yakoub.zine@utbm.fr

[1]UTBM, FEMTO-ST, FCLAB, CNRS, Belfort, France.

[2]Université de Franche-Comté, Institut Universitaire de France, UTBM, CNRS, FEMTO-ST, FCLAB, Belfort, France.

[3]ESTA, School of Business and Engineering, Belfort, France.

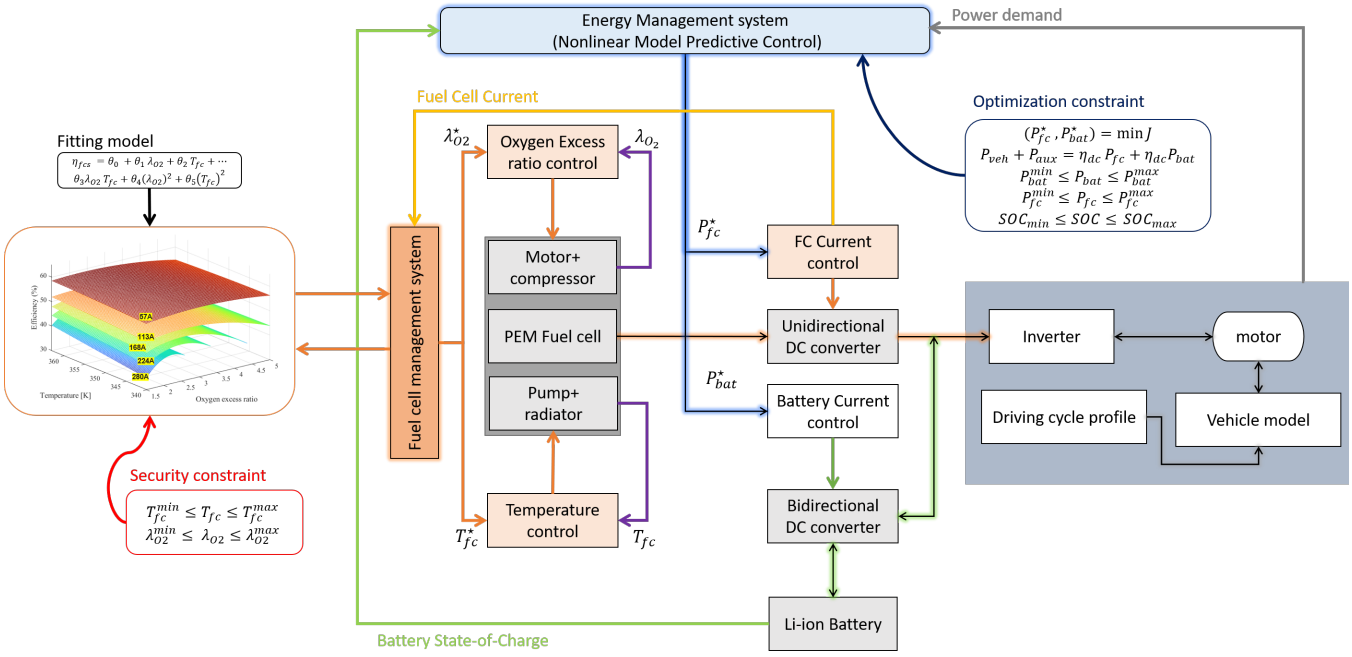

Fig. 1: Energy Management system based fuel cell management system general structure

A. Vehicle Modeling

As shown in Fig. 1, the powertrain of the vehicle under consideration comprises the FC as the primary power source and the Li-ion battery as a secondary source. Both sources must fulfill the total propulsion power (P_{veh}), which can be estimated based on the total forces (F_T) acting on the vehicle, its velocity (v), and the efficiencies of the electric motor ($\eta_m = 90\%$) and inverter ($\eta_i = 95\%$), using (1)

$$P_{veh} = \frac{F_T v}{\eta_m \eta_i} \tag{1}$$

where F_T is the sum of accelerating force (F_a), rolling force (F_r), drag force (F_d) and grading force (F_g), given as follows:

$$F_T = \underbrace{M_v \frac{dv}{dt}}_{F_a} + \underbrace{\gamma_r \rho_r M_v g \cos\theta}_{F_r} + \underbrace{M_v g \sin\theta}_{F_g} + \underbrace{\frac{1}{2}\rho_a \gamma_d S_v v^2}_{F_d} \tag{2}$$

where M_v is the vehicle mass, g is the gravity, γ_r is the rolling coefficient, θ is the road slop angle, ρ_a is the air density, γ_d is the drag coefficient, S_v is the vehicle chassis area.

The overall requested power (P_{req}) is determined by adding the vehicle's power needs to the power required by the auxiliary systems (P_{aux}) using (3)

$$P_{req} = P_{veh} + P_{aux} \tag{3}$$

where P_{aux} covers the power of the air supply system and thermal management system, and can be calculated as follows:

$$P_{aux} = P_{cm} + P_{pump} + P_{radiator} \tag{4}$$

where P_{cm}, P_{pump}, and $P_{radiator}$ represent the power consumed by the motor-compressor system, water pump, and radiator, respectively. These components are the primary auxiliary systems influencing the overall electric net power output.

B. Fuel Cell

The central component of the system is the FC stack, which facilitates the conversion of hydrogen and oxygen's chemical energy into electrical power. In the vehicle under investigation, a 65 kW FC stack is utilized, capable of producing currents of up to 310 A. This study focuses on three parameters that impact FC system performance:

1) ***Voltage****:* noted (V_{fc}), is approximated using a semi-empirical model to characterize the electrical behavior of the FC stack using (5)

$$\begin{aligned} V_{fc} = N_{cell}[E_{ocv} - (v_0 + v_1(1 - e^{-c_1 I_{fc}})) \\ - R_m I_{fc} - (c_2 \frac{I_{fc}}{i_{max}})^{c_3} I_{fc}] \end{aligned} \tag{5}$$

where N_{cell} denotes the number of FC cells (381), E_{ocv} represents the open-circuit voltage, $v_{\{0,1\}}$ are parameters related to activation loss, R_m stands for membrane resistance, $c_{\{1,2,3\}}$ denote semi-empirical coefficients, and i_{max} indicates the maximum current generated by the stack. For a thorough understanding of modeling and parameters, readers may refer to [14].

2) ***Temperature****:* Maintaining an optimal temperature is crucial for maximizing the efficiency of the stack. This involves regulating the cooling system, which comprises a water pump, radiator, and heater. Here, the temperature of the FC can be equated to that of the output water, with a temperature difference of approximately $5°C$ between the inlet and outlet. Given the control-oriented study, a simplified model for stack temperature (T_{fc}), can be derived based on the principle of mass conservation using (6)

$$M_{fc} C_{fc} \frac{dT_{fc}}{dt} = Q_{\text{produced}} - Q_{\text{water}} - Q_{\text{amb}} \tag{6}$$

where M_{fc} represents the mass of the FC stack (60 kg), C_{fc} denotes the specific heat of the stack ($710\ J/kg.K$), Q_{produced} signifies the heat generated by the stack, Q_{water} accounts for the heat absorbed by the water, and Q_{amb} indicates the heat released to the ambient environment, the heat absorbed by the gases is neglected in this study. These various quantities can be calculated based on (7)

$$\begin{aligned} Q_{\text{produced}} &= \left(\frac{N_{\text{cell}} \cdot M_{\text{H2}}}{2 \cdot F} \Delta H - V_{\text{fc}}\right) \times I_{\text{fc}} \\ Q_{\text{water}} &= \dot{m}_w \cdot C_w \cdot (T_{\text{fc}} - T_{\text{in}}), \quad Q_{\text{amb}} = k_1 \cdot (T_{\text{fc}} - T_{\text{amb}}) \end{aligned} \tag{7}$$

where M_{H_2} denotes the molar mass of hydrogen ($2\,\text{g/mol}$), ΔH is the hydrogen enthalpy ($285.5\,\text{kJ/mol}$), F is Faraday's constant ($96485\,\text{C/mol}$), $\dot{m}_w$ represents the water flow (the control variable of the cooling system, with a maximum flow of 3 L/min), C_w stands for the specific heat of water ($4200\,\text{J/kg.K}$), T_{in} indicates the inllet water temperature, k_1 denotes the stack radiation coefficient ($180\,\text{W/K}$), and T_{amb} represents the ambient temperature ($298.15\,\text{K}$). These parameters are derived from a scaling of the system investigated in [15].

3) ***Oxygen Excess Ration (OER)****:* denoted as λ_{O_2}, is pivotal for evaluating the oxidation reaction efficiency inside the FC. By optimizing λ_{O_2}, net power is maximized while operating issues related to oxygen starvation/saturation and excessive power consumption by the compressor motor system are avoided. The OER can be calculated as the ratio between absorbed oxygen ($W_{O_2}^{in}$) and reacted oxygen ($W_{O_2}^{react}$), as shown in (8)

$$\lambda_{O_2} = \frac{W_{O2}^{in}}{W_{O2}^{react}} = \frac{k_m x_{O2}(p_m - p_{ca})}{\frac{N_{\text{cell}} M_{O2} I_{\text{fc}}}{4F}} \tag{8}$$

where k_m is the supply manifold constant, x_{O2} is the oxygen fraction, p_m is the supply manifold pressure (Pa), p_{ca} is the cathode pressure (Pa), and M_{O2} is the oxygen molar mass ($32\ g/mol$).

To regulate the OER, we can derive a control-oriented model from the reduced-order model of the motor-compressor subsystem proposed in [16], as depicted in (9).

$$\dot{\omega}_{cp} = -m_1 \omega_{cp} - \frac{m_2}{\omega_{cp}} \left[\left(\frac{p_{ca}}{m_3} \right)^{m_4} - 1 \right] W_{cp}(\omega_{cp}, p_{ca}) + m_5 V_{comp} \tag{9}$$

where ω_{cp} is the angular velocity of the air compressor (rad/s), $W_{cp}(\omega_{cp}, p_{ca})$ represents the air flow rate through the compressor, $m_i\{i = 1, ..., 5\}$ are empirical parameters of the air supply subsystem and V_{comp} serves as the control signal representing the voltage supplied to the motor.

Finally, for a set of operating conditions $\{I_{fc}, T_{fc}, \lambda_{O_2}\}$, the efficiency of the FC system (E_{fcs}) is calculated using (10). This efficiency is defined as the ratio of the net electric power ($P_{net} = P_{fc} - P_{aux}$) to the chemical energy of hydrogen, along with the efficiency of the DC-DC boost converter, denoted as E_{dc}.

$$E_{fcs}(I_{fc}, T_{fc}, \lambda_{O_2}) = \frac{P_{fc} - P_{aux}}{LHV \times \dot{m}_{H2}} \cdot E_{dc} \tag{10}$$

where $\dot{m}_{H2}$ is the hydrogen mass flow rate (g/s), and is linearly proportional to the FC power, and LHV stands for low heating value of the hydrogen ($241.8\,kJ/mol$).

C. Battery:

In this study, Li-ion battery technology is used owing to its high energy density and low self-discharge rate. The battery's behavior is studied using an equivalent circuit model. This model helps understanding how the battery's state of charge (SOC) changes with power. The current integral method is employed to calculate the battery's SOC as (11)

$$\text{SOC}(t) = \text{SOC}(0) - \frac{\int_0^t I_{\text{bat}}(\tau)\, d\tau}{Q_n} \tag{11}$$

where SOC_0 is the initial SOC of the battery, Q_n is the rated battery capacity ($6.5\,Ah$), and I_{bat} battery charging/ discharging current which is calculated using

$$I_{bat} = \frac{V_{bat,ocv} - \sqrt{V_{bat,ocv}^2 - 4R_{bat}P_{bat}}}{2R_{bat}} \tag{12}$$

where $V_{bat,ocv}$, R_{bat} and P_{bat} are the battery's open-circuit voltage (V), equivalent resistance (Ω) and power (W), respectively.

III. EMS BASED FUEL CELL MANAGEMENT SYSTEM

A. Energy management system

NMPC-based EMS is used to allocate power between the two sources by using the plant model to predict the system behaviour and then improve future system performance by solving an optimal control problem at each sampling time. The plant prediction model as described in (12), revolves around a single state variable $x = SOC$, the control input of the plant is designated as $u = I_{fc}$, while the requested power and auxiliary power are assumed to be measurable disturbances ($d = P_{req}$). The discrete-time state-space formulation of the plant, with a sampling period of $\Delta T = 1s$, is expressed as given in equation (13).

$$x_{k+1} = x_k - \frac{V_{bat,ocv} - \sqrt{V_{bat,ocv}^2 - 4R_{bat}\left(\frac{d_k}{E_{dc}} - P_{fc}(u_k)\right)}}{2Q_n R_{bat}} \Delta T \tag{13}$$

In this study, a series of control inputs ($u_k = \{u(0), u(1), \ldots, u(N-1), u(N)\}$) is evaluated over a finite prediction horizon consisting of 10 samples (N=10), with the control horizon set equal to the prediction horizon for simplicity. The optimal length of the prediction horizon was established through simulations involving different N values, aiming to achieve an optimum compromise between computational cost and control performance. The NMPC EMS determines the optimal trade-off between the following performance metrics: hydrogen consumption ($\dot{m}_{H2}$), FC current variation ($\Delta I_{fc} = I_{fc}(k) - I_{fc}(k-1)$), and battery's SOC deviation from a predefined reference ($SOC - SOC_{ref}$). Thus, the rationalized cost function can be expressed as

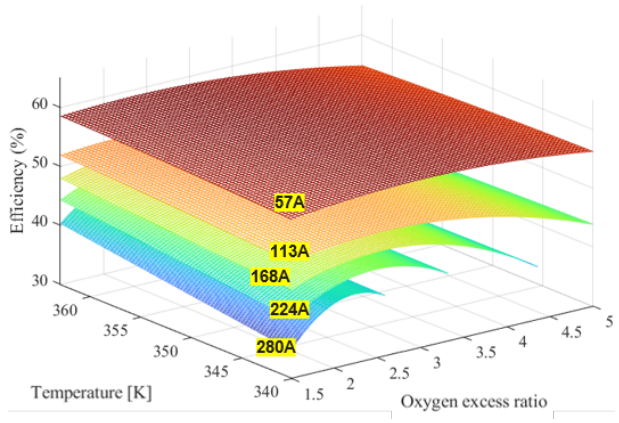

Fig. 2: Characterization of FC system for various current values: 57A, 113A, 168A, 224A, 280A.

follows:

$$\min_{u_k} J = \sum_{i=k}^{k+N-1} \left[\sigma_1 \left|\left| \frac{\dot{m}_{H2}}{\dot{m}_{H2}^{max}} \right|\right|^2 + \sigma_2 \left|\left| \frac{\Delta I_{fc}}{\Delta I_{fc}^{max}} \right|\right|^2 \right] + \sigma_3 \left|\left| \frac{SOC(k+N) - SOC_{ref}}{2(SOC_{max} - SOC_{max})} \right|\right|^2 \tag{14}$$

where $\dot{m}_{H2}^{max}$ is the maximum hydrogen mass flow rate (1.8 g/s), ΔI_{fs}^{max} is the maximum FC current variation (50 A), SOC_{ref} is the reference SOC set at 60%, SOC_{max} is the maximum SOC set at 80%, and SOC_{min} is the minimum SOC set at 45%, $\sigma_{\{1,2,3\}}$ are the weighting factors of the cost function.

In the optimization stage, the following constraints should be considered:

$$\begin{aligned} & E_{dc}P_{fc} + E_{dc}P_{bat} = P_{aux} + P_{veh} \\ & 45\% \leq \text{SOC} \leq 80\% \\ \text{subject to:} \quad & 0\,\text{kW} \leq P_{fc} \leq 70\,\text{kW} \\ & -20\,\text{kW} \leq P_{bat} \leq 20\,\text{kW} \\ & 0\,\text{A} \leq \Delta I_{fc} \leq 50\,\text{A} \end{aligned} \tag{15}$$

B. Fuel Cell management System

The FCMS serves as an intermediary control unit, producing temperature and OER references based on current inputs from the EMS. The process for designing the FCMS entails the following steps:

*1) **FC system characterization**:* To assess the efficiency of the FC system, an off-line simulation was carried. The characterization covered a range of operating conditions, including current varying from 5A to 280A, temperature from 340K to 363K, and OER fluctuations between 1.5 and 5. Fig. (2) illustrates the results for a set of current inputs.

*2) **Efficiency fitting model**:* For each value of the current, the efficiency can be expressed using the two variables second-order polynomial fitting model expressed in matrix form, as shown in (16)

$$E_{fcs,k}(T_{fc}, \lambda_{O_2}) = \underbrace{\begin{pmatrix} \xi_{1,1} & \xi_{1,2} & \cdots & \xi_{1,6} \\ \xi_{2,1} & \xi_{2,2} & \cdots & \xi_{2,6} \\ \vdots & \vdots & \ddots & \vdots \\ \xi_{N_{\text{test}},1} & \xi_{N_{\text{test}},2} & \cdots & \xi_{N_{\text{test}},6} \end{pmatrix}}_{\xi} \begin{pmatrix} 1 \\ T_{fc} \\ \lambda_{O_2} \\ T_{fc}\lambda_{O_2} \\ T_{fc}^2 \\ \lambda_{O_2}^2 \end{pmatrix}$$
$$\text{for all } k = \{1, \ldots, N_{\text{test}}\} \tag{16}$$

where N_{test} is the length of the test current set ($N_{test} = 55$), each row of the matrix ξ represents the the fitting parameters matrix for a single test current.

*3) **Optimal operating condition**:* Once the fitting model is established, the optimal references for both temperature ($T_{fc}^{\star}$) and OER ($\lambda_{O_2}^{\star}$) are derived by solving the system of equations shown in (17)

$$\begin{aligned} (T_{fc}^{\star}, \lambda_{O_2}^{\star}) = \min_{(T_{fc}, \lambda_{O_2}) \in \{\mathfrak{T}, \mathfrak{B}\}} & \begin{cases} \frac{\partial E_{fcs,\star}(T_{fc}, \lambda_{O_2})}{\partial T_{fc}} = 0 \\ \frac{\partial E_{fcs,\star}(T_{fc}, \lambda_{O_2})}{\partial \lambda_{O_2}} = 0 \end{cases} \\ \mathfrak{T}: \quad & T_{fc} \in [T_{fc}^{\min}, T_{fc}^{\max}] \\ \mathfrak{B}: \quad & \lambda_{O_2} \in [\lambda_{O_2}^{\min}, \lambda_{O_2}^{\max}] \end{aligned} \tag{17}$$

where $\{\mathfrak{T}, \mathfrak{B}\}$ represents the set of potential temperature and OER values, chosen to prevent potential faults: starvation ($\lambda_{O_2}^{\min} = 1.5$) and saturation ($\lambda_{O_2}^{\max} = 3.5$), and ensure operation within recommended temperature ranges from $T_{fc}^{\min} = 333\,K$ to $T_{fc}^{\max} = 363\,K$.

*4) **Operating condition control**:* Consequently, the operating conditions are controlled to track the obtained references using low-level control blocks. For simplicity, PID controllers are designed to facilitate implementation. The response times order for the electric, air supply system, and cooling system are about $\mathcal{O}(10^{-1})$ seconds, $\mathcal{O}(10^{-1})$ seconds, and $\mathcal{O}(10^{2})$ seconds, respectively.

IV. Results and Discussion

The proposed EMS underwent an evaluation using the Worldwide harmonized light vehicles test cycles (WLTC) cycle, a standardized protocol encompassing various driving conditions such as urban, suburban and highway scenarios. The primary findings of this test are depicted in Fig. 3, showcasing the driving cycle/power request (Fig. 3a), power allocation between the FC and battery (Fig. 3b), and certain performance metrics (Fig. 3c). From the results, the FC predominantly fulfills power demands, with the battery serving as a supplementary power source during peak periods. The total hydrogen consumption amounted to approximately 163 grams, resulting in an fuel consumption coefficient of $0.71\,kg/100\,km$.

The proposed EMS effectively stabilized the battery's SOC within the prescribed operational limits. Typically, an MPC-based EMS would ensure the final SOC value matches the reference. However, as shown in Fig. 3c, the final SOC is approximately 80%. This discrepancy can be attributed to the inherent characteristics of the extra-high phase of

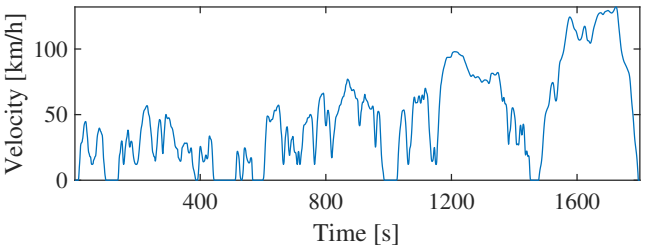

(a) WLTP driving cycle profile.

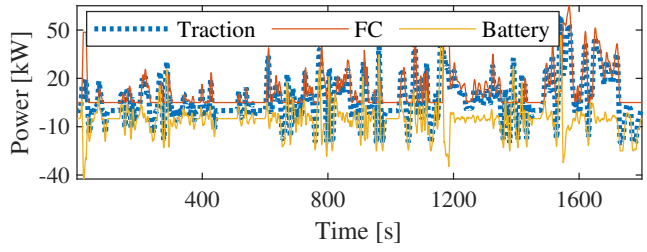

(b) Power sharing.

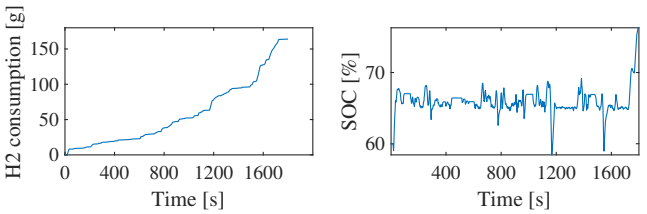

(c) Total hydrogen consumption and battery SOC variation.

Fig. 3: Results of NMPC Energy Management System

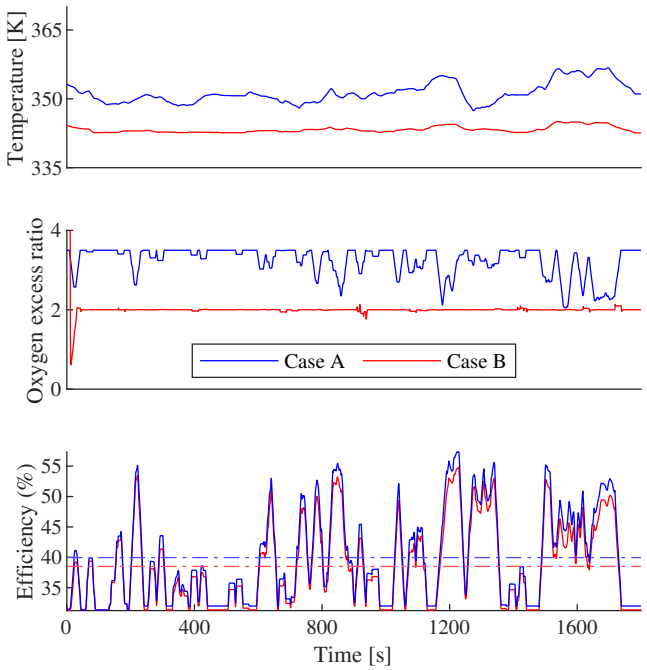

Fig. 4: Impact of variable operating conditions on FC System Efficiency: Case A - Optimal references vs. Case B - Fixed References

the WLTC driving cycle, where deceleration occurs. During this phase, the power demand is negative, and with the FC being irreversible and no regenerative braking available, all generated power is directed to the battery, resulting in an increase in the battery SOC.

To quantify the efficiency enhancement facilitated by the FCMS, we maintain identical power sharing settings of the EMS. Consequently, for identical current references, two distinct scenarios are compared. In Case A, the FCMS, elaborated in subsection III.B, dynamically adjusts temperature and OER references to optimize FC performance. Conversely, Case B employs manually fixed references: a temperature reference of 345K and an OER reference of 2. Fig. 4 depicts the measured operational conditions and the corresponding variations in overall FC system efficiency for both cases. The efficiency curves reveal distinct enhancements across varying power consumption levels. Notably, efficiency improvements range from approximately 1-2% at low power demands, escalate to around 2-3% at medium power demands, and peak at up to 4% for high power demands. When considering the mean efficiency, represented in dashed lines, across the WLTC driving cycle, our analysis reveals an improvement of about 1.5%/cycle. Table I offers a comprehensive analysis of efficiency enhancements across various driving conditions, demonstrating that the implemented FCMS notably improves efficiency, especially in medium to high power ranges.

V. Conclusion

This study investigated the integration of the FCMS into the EMS of a FCHEV to evaluate and quantify efficiency enhancement. A model encompassing the FC stack, the auxiliaries (air supply/cooling), and the battery was developed. An NMPC-based energy management system was established for power allocation. Lastly, an offline characterization-based FCMS was deployed. The FCHEV system was simulated under a complete WLTC driving cycle considering two scenarios: optimal and fixed operating conditions (temperature, oxygen excess ratio). The results demonstrated that the optimal FCMS enhanced the FC system efficiency by up to 4% compared to the scenario with fixed operating conditions.

Future work can extend this research by incorporating FC dynamics to refine the model's accuracy and operational responsiveness. Additionally, examining the degradation effects on both the FC and the battery could provide deeper insights into the long-term performance and reliability of the FCHEV system.

Acknowledgment

This work has been supported by the EIPHI Graduate School (contract ANR-17-EURE-0002) and the Region Bourgogne Franche-Comté.

VI. Appendix

Table II outlines the simulation parameters utilized to derive the results presented in this study.

TABLE I: FCHEV system efficiency improvement across various driving scenarios.

Driving Scenario	Time Span (s)	Max Speed (km/h)	Mean FC Power (W)	Peak Efficiency (%)		Mean Efficiency (%)	
				Case A	Case B	Case A	Case B
City	0-600	56.6	25,818.2	59.32	56.52	36.31	35.67
Suburban	600-900	76.6	37,522.7	59.85	57.56	42.85	41.25
Rural	900-1500	97.4	45,992.6	60.74	57.46	40.82	39.44
Highway	1500-1800	131.3	56,800.3	60.49	57.61	44.03	41.06

TABLE II: Vehicle Parameters Description and Values.

Component	Parameter	Value
Vehicle	Mass (kg)	1950
	Frontal area (m^2)	2.1
	Air density (kg/m^3)	1.202
	Rolling coefficient	0.0015
	Drag coefficient	0.29
	Gravity acceleration (m/s^2)	9.81
	Inverter efficiency (%)	90
	Motor efficiency (%)	90
Fuel Cell	Type	PEMFC
	Rated power (kW)	65
	Number of cells	381
	Maximum current (A)	310
Battery	Type	Li-ion
	Capacity (Ah)	6.5
	Nominal voltage (V)	245
	Internal resistance (Ω)	0.019

REFERENCES

[1] L. Zhu, F. Tao, Z. Fu, H. Sun, B. Ji, and Q. Chen, "Multiobjective optimization of safety, comfort, fuel economy, and power sources durability for fchev in car-following scenarios," *IEEE Transactions on Transportation Electrification*, vol. 9, no. 1, pp. 1797–1808, 2022.

[2] Y. Zhou, A. Ravey, and M.-C. Pera, "Operational cost analysis of fuel cell electric vehicles under different powertrain-sizing configurations," in *2020 IEEE Vehicle Power and Propulsion Conference (VPPC)*. IEEE, 2020, pp. 1–6.

[3] H. Li, A. Ravey, A. N'Diaye, and A. Djerdir, "A review of energy management strategy for fuel cell hybrid electric vehicle," in *2017 IEEE Vehicle Power and Propulsion Conference (VPPC)*. IEEE, 2017, pp. 1–6.

[4] A. M. Fernandez, M. Kandidayeni, L. Boulon, and H. Chaoui, "An adaptive state machine based energy management strategy for a multi-stack fuel cell hybrid electric vehicle," *IEEE Transactions on Vehicular Technology*, vol. 69, no. 1, pp. 220–234, 2019.

[5] H. Li, Y. Zhou, H. Gualous, H. Chaoui, and L. Boulon, "Optimal cost minimization strategy for fuel cell hybrid electric vehicles based on decision-making framework," *IEEE Transactions on Industrial Informatics*, vol. 17, no. 4, pp. 2388–2399, 2020.

[6] A. Bäumler, A. Benterki, M. Jianwen, A. Toufik, and M. Boukhnifer, "Energy management strategy based on reinforcement learning for fuel cell hybrid vehicle with a new reward function approach," in *2023 IEEE Vehicle Power and Propulsion Conference (VPPC)*. IEEE, 2023, pp. 01–06.

[7] B. Liu, C. Sun, X. Wei, D. Wen, C. Ning, and H. Li, "Guided eco-driving of fuel cell hybrid electric vehicles via model predictive control," in *2023 IEEE Vehicle Power and Propulsion Conference (VPPC)*. IEEE, 2023, pp. 1–6.

[8] D. F. Pereira, F. da Costa Lopes, and E. H. Watanabe, "Nonlinear model predictive control for the energy management of fuel cell hybrid electric vehicles in real time," *IEEE Transactions on Industrial Electronics*, vol. 68, no. 4, pp. 3213–3223, 2020.

[9] X. Lü, S. Li, X. He, C. Xie, S. He, Y. Xu, J. Fang, M. Zhang, and X. Yang, "Hybrid electric vehicles: A review of energy management strategies based on model predictive control," *Journal of Energy Storage*, vol. 56, p. 106112, 2022.

[10] R. Mezzi, N. Y. Steiner, M.-C. Pera, D. Hissel, and L. Larger, "Operating conditions control for extending proton exchange membrane fuel cell lifetime," in *2017 IEEE vehicle power and propulsion conference (VPPC)*. IEEE, 2017, pp. 1–6.

[11] J. Chen, Z. Liu, F. Wang, Q. Ouyang, and H. Su, "Optimal oxygen excess ratio control for pem fuel cells," *IEEE Transactions on control systems technology*, vol. 26, no. 5, pp. 1711–1721, 2017.

[12] L. Yin, Q. Li, E. Breaz, W. Chen, and F. Gao, "Net power enhancement of pemfc system based on dual loop multivariable coordinated management," *IEEE Transactions on Industrial Electronics*, 2023.

[13] X. Ge, K. Li, W. Tian, R. Wang, X. Wan, and H. Tang, "Efficiency improvement strategy of fuel cell system based on oxygen excess ratio and cathode pressure two-dimensional optimization," *International Journal of Hydrogen Energy*, vol. 57, pp. 136–147, 2024.

[14] J. T. Pukrushpan, A. G. Stefanopoulou, and H. Peng, *Control of fuel cell power systems: principles, modeling, analysis and feedback design*. Springer Science & Business Media, 2004.

[15] Z. Liu, J. Chen, L. Kumar, L. Jin, and L. Huang, "Model-based decoupling control for the thermal management system of proton exchange membrane fuel cells," *International Journal of Hydrogen Energy*, vol. 48, no. 50, pp. 19 196–19 206, 2023.

[16] R. J. Talj, D. Hissel, R. Ortega, M. Becherif, and M. Hilairet, "Experimental validation of a pem fuel-cell reduced-order model and a moto-compressor higher order sliding-mode control," *IEEE Transactions on Industrial Electronics*, vol. 57, no. 6, pp. 1906–1913, 2009.